Evidence of Attenuation of VHE Blazar Spectra by Extragalactic Background Light

Cameron Allen
Advisor: Dr. Jodi Christiansen
Cal Poly Physics Department
2015

ABSTRACT

The spectrum of two blazar objects, 1ES 1959+650 and 1ES 2344+514, are analyzed for evidence of interactions with the Extragalactic Background Light (EBL), using combined data from the Very Energetic Radiation Imaging Telescope Array System and the Fermi Gamma-ray Space Telescope, By analyzing the distinct curvature across the combined spectrum, we infer that the very-high energy (VHE) gamma-rays must be attenuated by interactions with the EBL. We also find that the measured 1ES 1959+650 spectrum is sensitive to the intrinsic blazar model, with a preference for a power-law with an exponential cutoff (EPWL). The measured curvature is a combination of the EBL attenuation and the exponential cut-off, as determined by statistical tests assuming that there is no EBL. Finally, a test of the optical depth due to the EBL indicates that the two blazars are consistent with the amount of EBL given by the Franceschini model of intergalactic optical depth.

TABLE OF CONTENTS

INTRODUCTION

In the late 1950s, scientists discovered radio sources that were associated with previously observed objects that appeared to be stars or galaxies based on their visual qualities. Based on the hydrogen Balmer series and magnesium emission lines, it was deduced that these objects were extragalactic and extremely luminous. The 'quasi-stellar' objects were particularly disturbing because did not fit into any existing stellar model. This new class of sources was given the name 'quasar. By 1965, these quasars were found to be strong x-ray emitters. This implied new physics that results from non-thermal processes. Today quasars are believed to be just a sub-type of a larger category called Active Galactic Nuclei (AGN). All AGNs are characterized by a bright galactic core that is often brighter than the host galaxy, and emit radiation across the entire electromagnetic spectrum. Theorized to be the result of the accretion of matter around a supermassive black hole at the center of the galaxy, the geometry and orientation of these active galaxies determines what sort of physics we can study and what sort of radiation we can observe. The Unified AGN Model, displayed in Figure 1, explains the various types of AGNs based on our viewing angle. Common to many AGNs are massive relativistic jets that shoot out of the poles of the black hole, perpendicular to the accretion disc. If the AGN happens to be oriented such that this jet is pointed at Earth, we call it a blazar.

Blazars are amongst the most energetic objects in the Universe, most directly due to the observed physics of the relativistic jet. With our vantage point in line with the jet, we observe Synchrotron Self-Compton Radiation. This phenomenon is the primary source of both x-rays and very-high energy (VHE, E > 100 GeV) gamma-rays emitted from the blazar. The x-rays are the result of the synchrotron radiation and the VHE gamma-rays are the result of the inverse-Compton Effect shown in Figure 2 below. As electrons are accelerated down the relativistic jet they emit synchrotron radiation in the form of x-rays. These electrons then strike the synchrotron x-rays they just emitted and transfer their energy to the photons through the inverse-Compton Effect. Combined with the highly relativistic speed of the jet itself, these energized photons come to Earth as VHE gamma-rays. On occasion, blazars will 'flare', wherein the emitted flux jumps to a much higher value for a short period of time, before returning to its normal value. This effect is believed to be due to clumps of electrons sporadically injected into the jet from the central engine. It is a side effect of these gamma-rays that blazars have very weak, if any, emission or absorption spectral lines, making any sort of redshift or distance calculation much more difficult than it is for other AGNs.

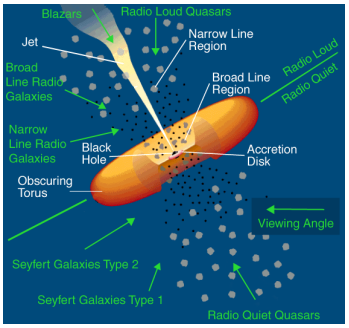

Figure 1: The Unified AGN Model characterizes an AGN based on its orientation in relation to Earth and our viewing angle.

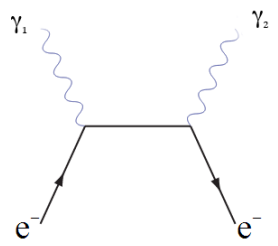

Figure 2: Diagram of Inverse Compton Effect. An electron interacts with a lower-energy photon γ_1 and imparts energy to it, turning it into a gamma-ray photon γ_2.

While the study of blazars in and of themselves is a fascinating topic in physics, they also contribute to the further understanding of many related topics in astrophysics. The focus of this paper is to learn more about the Extragalactic Background Light (EBL) and its interactions with VHE gamma-rays. Similar to the Cosmic Microwave Background (CMB), the EBL is the sum total of all ultraviolet, optical, and infrared light produced by galaxies and stars [1]. Much like studying the CMB leads to clues about the evolution of the Universe, the study of the EBL compliments and expands on research regarding galaxy formation and evolution. It is theorized that the EBL is distributed throughout the radius of causality of stars. While newer stars are more like point sources and their light has not gone as far out, when we consider objects of redshift ~ 10 there is little difference between the light in one location or another. If most of the starlight was emitted during the early periods of star and galaxy formation, then the distribution locally is expected to be more or less uniform.

There is an intrinsic challenge in measuring the EBL as it is drowned out by the local, zodiacal light that we see due to our close position to the Sun. This means direct measurements of the EBL are impossible to perform. However, the photons in the EBL interact with the VHE gamma-ray photons in the blazar jet via pair-production processes, which results in attenuation of the VHE gamma-ray beam. The purpose of this research into EBL attenuation is to determine to what extent the attenuation affects the spectrum.

OBSERVATORIES

Earth's atmosphere presents a challenge for observing gamma-ray sources because although optical light passes through it easily, it blocks out most other forms of electromagnetic radiation, including gamma-rays. There are a couple of ways to resolve this issue, but they all rely on the same basic principle of scintillation detection. The analysis in this paper utilizes data from two different observatories: the ground-based Very Energetic Radiation Imaging Telescope Array System (VERITAS) that observes high-energy particle showers in the atmosphere, and the Fermi Gamma-ray Space Telescope that observes nearly 20% of the sky at all times from orbit. Each telescope observes the same objects in a variation of scintillation detection. In the case of VERITAS, the atmosphere acts as the scintillation medium, while Fermi has a series of plastic layers that are the scintillators. The two observatories operate in different energy ranges, and by combining the results of both we observe a

greater portion of a source's spectrum and can clearly see any attenuation in the VHE regime. The ideal analysis uses contemporaneous data from VERITAS and Fermi, or data taken during the same period of time. This accounts for any flaring in the source that might occur, so both observatories are working with data that can be compared.

VERITAS

Located in southern Arizona at the Fred Lawrence Whipple Observatory, VERITAS is a telescope array that is dedicated to VHE gamma-ray observations and is operated by an international collaboration of astrophysicists and astronomers. Each of the four telescopes is of the Davies-Cotton imaging Cherenkov telescope design. A Davies-Cotton telescope uses an array of mirror plates in place of one large mirror. Each plate focuses at half the distance of the overall telescope focus, which allows the telescope to have a large aperture in relation to its focal length. These telescopes are 12 meters in diameter, use 350 hexagonal mirror plates, and focus on a collection of 499 photomultiplier tubes (PMT) [2]. To account for gamma-rays being blocked from reaching the ground by the atmosphere, VERITAS observes the interactions of these gamma-rays in the upper atmosphere. As shown in Figure 3, VHE gamma-rays that strike the atmosphere cause pair-production of electrons and positrons. These electrons and positrons have such high energy that they travel faster than the local speed of light, and excite other atoms in the atmosphere. As these excited atoms drop back down to their ground state, they emit a faint blue light known as Cherenkov radiation. The initial electrons and positrons continue to strike other particles in the atmosphere and energize them as well, and the end result is a large cone of light (ground radius ~ 130m, height ~ 10 km) of distinct, albeit brief, blue light [2].

The Imaging Atmospheric Cherenkov Technique (IACT) uses Cherenkov radiation to image the air shower. VERITAS uses IACT to make all of its observations. With four telescopes, VERITAS observes these showers from slightly different angles, and each telescope's image is used to reconstruct the gamma-ray direction using stereoscopy.

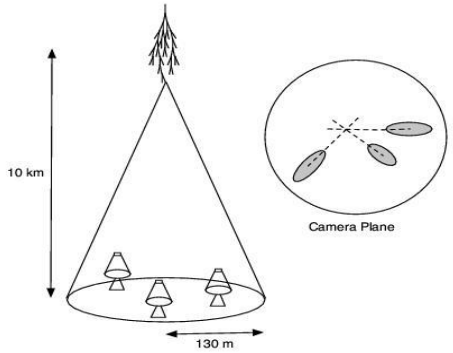

Figure 3: Illustration of a Cherenkov radiation shower, showing how the event appears when all the telescopes' results are merged.

FERMI

The Fermi Gamma-ray Space Telescope is the most recent gamma-ray space observatory, launched in 2008 by NASA to provide information on high-energy (10 keV – 300 GeV) gamma-rays. Fermi has two main instruments that compliment VERITAS, the Large Area Telescope (LAT) and the Gamma-ray Burst Monitor (GBM), though the majority of the collaborations with VERITAS are performed with the LAT [3].

The LAT is comprised of a 4x4 array of 'towers' that consist of a tracker, calorimeter, and data acquisition module, all of which are covered by an anticoincidence shield and conversion foils. A diagram of one of these towers is shown in Figure 4, and is in function similar to the technology used in particle detectors [3]. As gamma-rays pass through the anticoincidence shield and the conversion foils, the gamma-rays pair-produce into electrons and positrons. Determining the source location of these gamma-rays is dependent upon the energy and momentum of the produced particles. The energy of these particles is proportional to the shower created and is measured by the calorimeter, and the magnitude of the momentum can be found knowing the mass of each particle. The direction of the source is then reconstructed from the particle tracks and the principle of conservation of momentum.

OBSERVATIONS

VERITAS

The VERITAS observations were analyzed by running the collaboration's VEGAS software package v 2.5.4rc1. VEGAS is a multi-stage process that takes the raw data from the four telescopes and reconstructs the blazar's location and spectrum. The six stages of VEGAS each build on the previous stage, but can otherwise be run independently. This allows us to analyze the data in a variety of methods without having to run calibration each time.

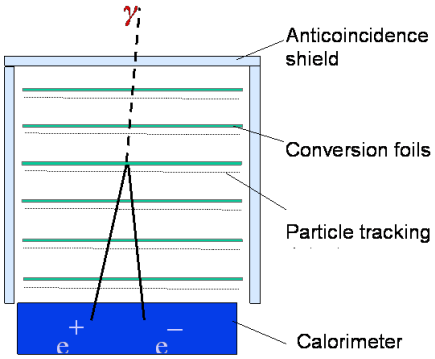

Figure 4: Fermi LAT tower detector diagram. By reconstructing the paths of created electrons and positrons, Fermi can pinpoint the source location in space.

- Stage 1 performs the calibration calculations for the analysis. In this stage, the hardware dependent qualities of the observations are input so that the analysis takes into account factors such as gain, timing, and bad channels in the PMTs. These calibrations are applied to both test laser data as well as source data.

- Stages 2 and 3 are combined, and take the calibrations calculated by Stage 1 for the PMTs and apply it to all the source data. They run in a similar manner to Stage 1, but this time compare the observed data to the calibration laser file. In addition, Stage 3 also determines the Hillas parameters that describe each telescope's image of the air shower. These parameters define an ellipse around each image in terms of centroid position in two dimensions, length and width, the orientation angle, and the size, which is a parameter proportional to the integrated number of Cherenkov photons.

- Stage 4 is responsible for reconstructing the gamma-ray direction. This stage is run using a choice of cuts, which are additional parameters that are chosen to cut out data that is bad or due to backgrounds. VEGAS analysis is optimized with predetermined 'soft,' 'medium,' or 'hard' cuts depending on the proportion of low energy to high-energy events. The analysis in this paper was performed with the default medium cuts: the distance between the center of the camera and image centroid was less than 1.43 degrees, and the image size was greater than 400 for data collected before 2012 and the image size was greater than 700 for data collected after 2012 when the camera was upgraded. Stage 4 then produces a stereo reconstruction of the gamma-ray from all four telescopes.

- Stage 5 applies additional cuts to the Stage 4 stereo reconstruction, to make the file size more manageable.

- Stage 6 is the final stage and calculates the significance of gamma-ray events coming from the source location. It also reconstructs the energy spectrum of the source. The sky map and spectrum are shown in Figure 5 and for 1ES 2344+514 in Figure 6. More cuts are applied to enhance the significance: the 'On' region was defined by gamma-ray directions within a 0.1 degree radius circle around the source, the mean scaled length of the Hillas parameters between 0.05 – 1.3, the mean scaled width of the Hillas parameters between 0.05 – 1.1, and the height of the maximum brightness of the air shower is above 7 km.

Significance is an important part of the blazar analysis, as it determines whether or not the observations are detections that are inconsistent with the background. The stage 6 analysis calculates the significance and background based on the Ring Background Model (RBM) method devised by Berge *et al*.[4]. The RBM method is a background-subtraction process where a ring around the source is integrated to determine the background flux, and then scaled and subtracted from the flux near and on the source. The difference, termed the excess, is our estimate of the signal. The significance of the signal is the number of standard deviations between the excess flux and the average background flux. Traditionally, if a significance of greater than 5σ is found, the source is considered detected. In Figure 5,

the sky map for 1ES 1959+650 reaches a source excess of 32.8 standard deviations. In Figure 6 the sky map for 1ES 2344+514 reaches a source excess of 23.3 standard deviations.

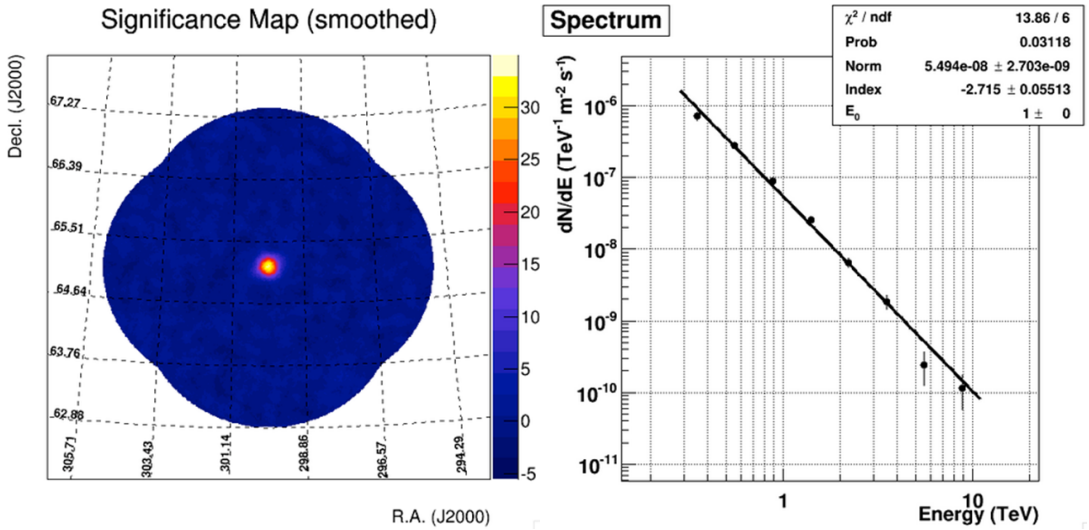

Figure 5: Examples of the output of VEGAS Stage 6, for 1ES 1959+650. A sky map (left) takes the observations from the four telescopes and plots the significance as a function of position. A sample spectrum (right) shows the flux of the source as a function of the energy of the gamma-rays, which are binned and then fit by different models.

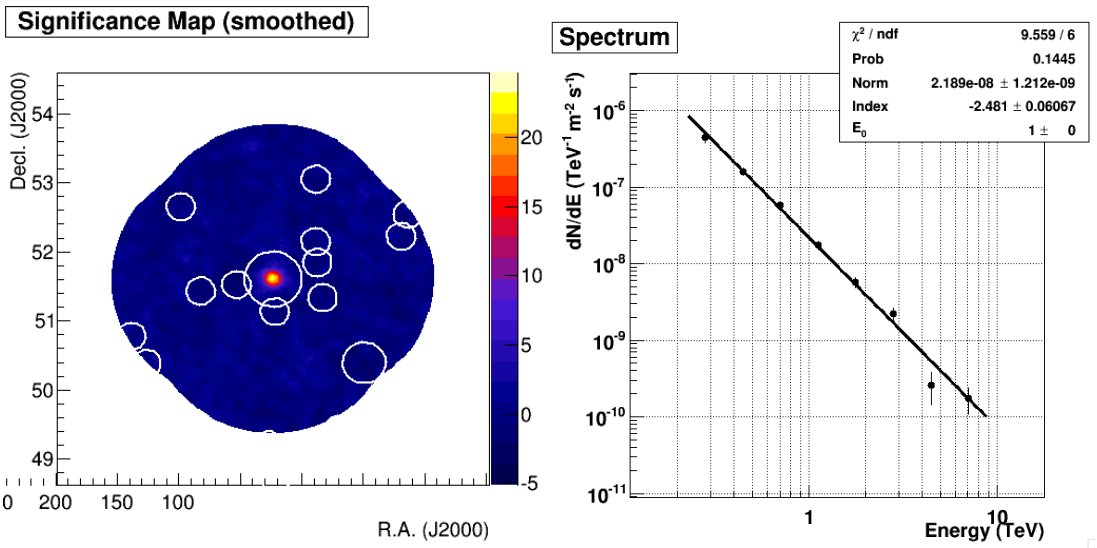

Figure 6: Examples of the output of VEGAS Stage 6, for 1ES 2344+514. The sky map (left) has numerous circles on it indicating the regions were stars were in the observations, and ultimately removed. The spectrum (right) again displays the flux as a function of energy.

FERMI

The Fermi observations were taken during a similar time period as the VERITAS observations to ensure that flaring in the blazar isn't present in one data set and not in the other. Figure 7 shows the data obtained from collaborators working on Fermi, in a "butterfly" or "bowtie" format. The Fermi bowtie was based on the maximum uncertainty in the spectral flux and index (slope) of a power law model. The shape encompasses all possible combinations of flux and index consistent with the data. The narrowest point, or the waist, is the point where the uncertainty in the index is at a minimum, and the only uncertainty is in the flux. To perform the fits and analysis required, we created sample points that lie within this bowtie as guides. Each point is a potential data point given the error limits provided by Fermi. For 1ES 1959+650, we chose five sample points that were spaced far enough apart to avoid issues with VERITAS overlap, while for 1ES 2344+514, with its smaller energy range, we chose four sample points.

EBL ANALYSIS

The physical parameters of 1ES 1959+650 and 1ES 2344+514 are found in Table 1. Both sources are relatively near to Earth, having a redshift that is comparatively small, and they both occupy the same hemisphere of the sky. 1ES 1959+650 is the stronger source of the two, with a much higher flux output as measured in Crab Units (CU). A Crab Unit is the intensity from the Crab Nebula above a specified threshold energy.

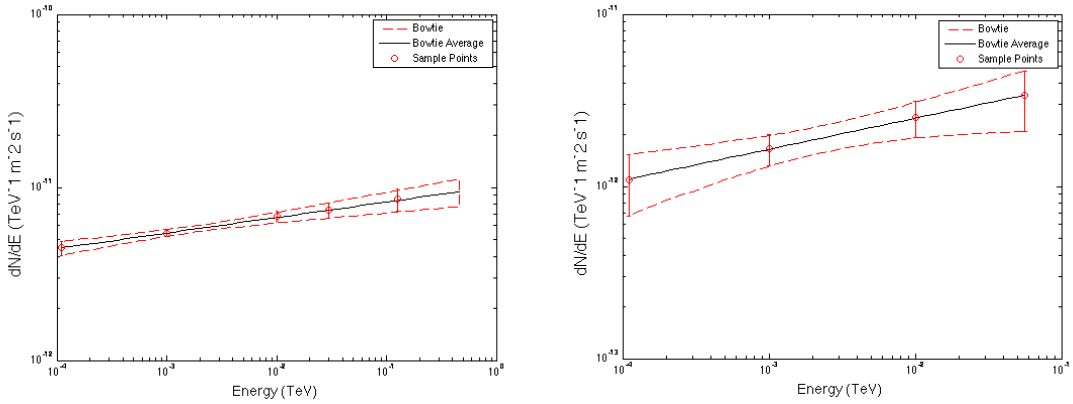

Figure 7: Contemporaneous Fermi bowtie data for 1ES 1959+650 (left) and 1ES 2344+514 (right). The 1ES 1959+650 data spans a greater energy range, allowing for five sample points, while 1ES 2344+514 uses four.

Source	Redshift z	RA (h m s)	Dec (degrees)	Flux
1ES 1959+650 [5]	0.048	19 59 59.9	+65 08 54	0.64 CU above 600 GeV
1ES 2344+514 [6]	0.044	23 47 04.9	+51 42 17	0.11 CU above 350 GeV

Table 1: Summary of the information on each source.

MODELLING METHODS

The analysis performed here is based upon the methods utilized by the H.E.S.S. Collaboration [7], which was heavily based upon the optical depth model of Franceschini *et al*.[8]. We assume the flux observed by VERITAS and Fermi is diminished as a result of interactions with the EBL, which we describe with exponential absorption:

$$\phi_{meas}(E,z) = \phi_{int}(E)e^{-\alpha\tau(E,z,n)} \quad (1)$$

where ϕ_{meas} is the observed spectral flux we see, ϕ_{int} is the intrinsic spectral flux of the source, α is a normalization factor (initially set to 1) of optical depth, and τ is the optical depth of the Universe based upon the Franceschini model with a photon density n, redshift z, and photon energy E. With this information it is possible to look solely at the intrinsic, de-absorbed spectrum by dividing the measured spectrum by the exponential absorption:

$$\phi_{int}(E) = \phi_{meas}(E,z)e^{\alpha\tau(E,z,n)} \quad (2)$$

The attenuation in the blazar spectrum is noticeable in the VHE regime but is negligible at the Fermi energies. Any model of the total VHE blazar spectrum must be able to fit both the Fermi data and the diminished flux in the VERITAS data. We investigated the three models shown in Table 2 to best determine which accurately describes the physical mechanisms of the blazar jet. The PWL model parameters are the Normalization flux, ϕ_0, the index, Γ, and a fixed parameter, E_0 = 1 TeV. The EPWL has an additional parameter for the cut-off energy, E_{cut}. The LP model replaces Γ with the parameter a, and introduces a new logarithmic term with parameter b. On a logarithmic plot, the PWL model is a straight line, the EPWL model is a straight line and then curves down at the cut-off energy E_{cut}, and the LP model has curvature everywhere.

Model	Function (ϕ_{int})
Power Law (PWL)	$\phi_0(E/E_0)^{-\Gamma}$
Power Law with Exponential Cut-off (EPWL)	$\phi_0(E/E_0)^{-\Gamma}e^{-(E/E_{cut})}$
Log-Parabola (LP)	$\phi_0(E/E_0)^{-a-b\,log(\frac{E}{E_0})}$

Table 2: Models used to analyze combined Fermi and VERITAS data.

ANALYSIS

We began by fitting each of the three models to the combined data for each source. To better visualize the difference between the Fermi and VERITAS data, we multiplied all flux values by E^2 and plotted the residuals of the fit. Additionally, to account for a systematic flux variation between VERITAS and Fermi, we multiplied the VERITAS data by a flux normalization factor. The flux normalization for both 1ES 1959+650 and 1ES 2344+514 was set to 0.8. The results for 1ES 1959+650 are shown in Figure 8, and the results for 1ES 2344+514 are shown in Figure 9. Each model is fit to the de-absorbed combined VERITAS and Fermi spectrum data on a logarithmic plot of $E^2\phi_{int}\ (TeV\ m^{-2}\ s^{-1})$ vs $E\ (TeV)$, although the actual measured spectrum for VERITAS is also shown in each plot. The large bowtie represents the Fermi data, the blue data points represent the spectrum as seen by VERITAS, and the green points are the VERITAS data accounting for EBL attenuation, and are thus have greater flux than the blue points. The Fermi bowtie has already been fit to a power law for these two sources, which is why it is straight rather than having any curvature. All fitting was performed in MatLab using a Marquardt-Levenberg method.

For 1ES 1959+650, it is immediately evident that the EPWL model agrees with the data better than the other models. The Fermi bowtie is straight and has high precision with its relatively small error bars, while the VERITAS data has a large curve in it, as discussed above. Neither the PWL model nor the LP model is able to account for the curvature of the combined spectrum. The PWL model is too straight in the VERITAS range, while the LP model is restricted in its curvature by the low energy Fermi sample points.

Performing a similar analysis for 1ES 2344+514 yields similar results, but with less statistical precision. Unlike 1ES 1959+650, where there is a clearly preferable model, the same cannot be said as strongly for 1ES 2344+514. Though the EPWL model is able to best match the long straight Fermi portion of the spectrum as well as the curvature in the VERITAS portion, the greater uncertainties in the Fermi data allow for more curvature in the LP model, to the point that it nearly matches the data, albeit very roughly.

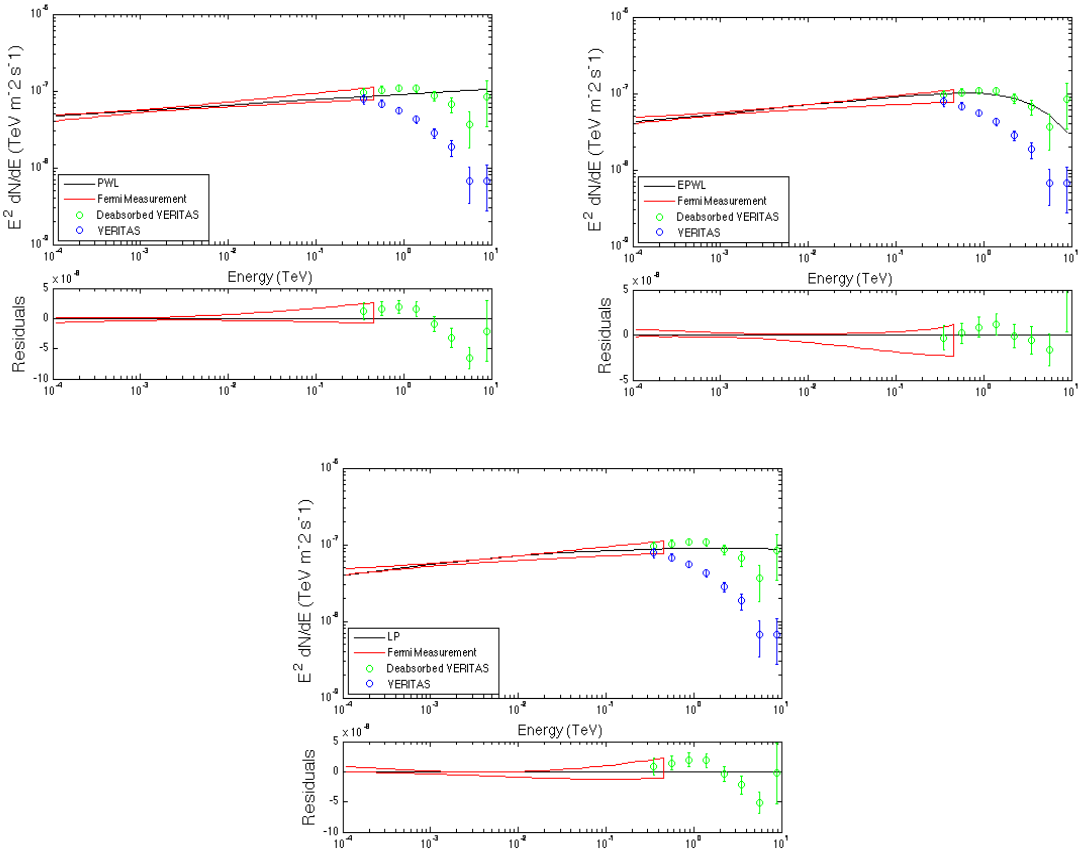

Figure 8: Fitted Models of 1ES 1959+650. PWL (top left), EPWL (top right), and LP (bottom).

The discrepancy in the analysis is due to two factors: 1) the precision of the Fermi data is much higher for 1ES 1959+650 than it is for 1ES 2344+514, leading to much tighter fitting results, and 2) there is overlap between VERITAS and Fermi data for 1ES 1959+650 that does not exist for 1ES 2344+514, i.e. the additional sample point in the Fermi set for 1ES 1959+650 helps constrain the fit.

To claim a statistical truth rather than merely noticing visual quality of the agreement, we proceeded to determine the χ^2 and p-values of each model based on the fit to the de-absorbed spectrum. The χ^2 values are related to the goodness of fit for each model, while the degrees of freedom (D.O.F) represent how many data points are involved in the fit. The p-value describes how probable the model is based on the χ^2 and D.O.F values. A good model would theoretically have a small χ^2 value and a high p-value. Table 3 summarizes these statistical values for both 1ES 1959+650 and 1ES 2344+514. Confirming the visual conclusion, the EPWL is the most likely model for both sources, but it is only statistically consistent ($p > 90\%$) with the blazar spectrum for 1ES 1959+650 based upon the χ^2 values.

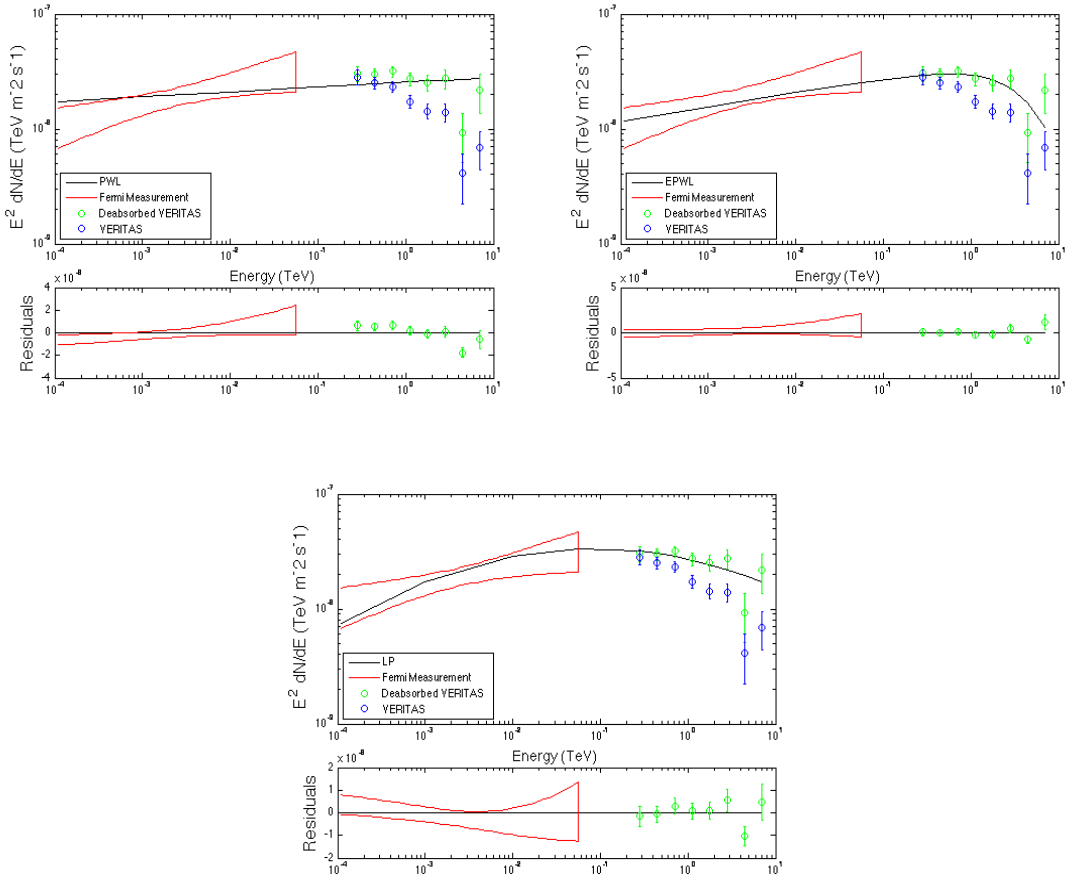

Figure 9: Fitted Models of 1ES 2344+514. PWL (top left), EPWL (top right), and LP (bottom).

Source	Model	X^2/D.O.F	p-value
1ES 1959+650	PWL	72.4 / 11	< 0.01 %
	EPWL	2.2 / 10	99.46 %
	LP	33.2 / 10	< 0.03 %
1ES 2344+514	PWL	30.0 / 10	0.09 %
	EPWL	7.9 / 9	54.43 %
	LP	9.3 / 9	41.01 %

Table 3: Fitted Model statistics for 1ES 1959+650 and 1ES 2344+514 with $\alpha = 1$.

However, the measured curvature is a combination of the EBL attenuation and the exponential cut-off. To determine the extent to which the EBL causes the curvature in the spectrum, we also performed a χ^2 test on the spectrum with the EPWL model assuming there was no EBL absorption, finding χ^2 /D.O.F = (52.2/ 10), p < 0.01% for 1ES 1959+650 and χ^2 /D.O.F = (41.6/9), p < 0.01% for 1ES 2344+514. Seeing how the EPWL on its own is just as poor as the PWL or LP models, we can say that EBL attenuation is an important factor in the curvature of the spectrum.

From there, we attempted to see how the models fared if we altered the normalization factor α, which models the EBL intensity through intergalactic optical depth. Initially the analysis was performed with α = 1, but that was an arbitrary value chosen to follow the Franceschini model exactly. To find the best value, we ran the model fitting process with a series of 300 values between α = 0.01 and α = 3, and found the χ^2 at each. The results are shown below in Figure 10, and confirm that the EPWL model is the best model statistically in the whole region. Based on the results found by the H.E.S.S. collaboration, where they determined $\alpha = 1.27^{+\ 0.18}_{-\ 0.15}$ [7], we constrained the data to fall within 2σ of this value (0.97 < α < 1.63). We found the minimum χ^2 for each model in each source within this range, and the final results are shown in Table 4.

In addition to the range given by H.E.S.S., we looked at the limits of the data itself, without filter or constraints. Over the whole range of α, from 0.01 to 3, we found the minimum value for χ^2 for each source, and then found the reduced χ^2 values (χ^2/D.O.F = χ^2_{red}). To determine the error in α, we let δα be the distance between α_{min} at $\chi^2_{min,red}$ and α at $\chi^2_{min,red}$ + 1. For 1ES 1959+650, fit to the EPWL model, we found that $\alpha = 0.86^{+1.36}_{-0.86}$ while 1ES 2344+514, also fit to the EPWL model, has $\alpha = 1.18^{+1.79}_{-1.18}$. The full results of this analysis for all models are tabulated in Table 5. Due to the wide basin in the LP model for 1ES 2344+514, we were unable to measure its uncertainty. Based on this analysis, we conclude that the results for the EPWL are consistent with the Franceschini model.

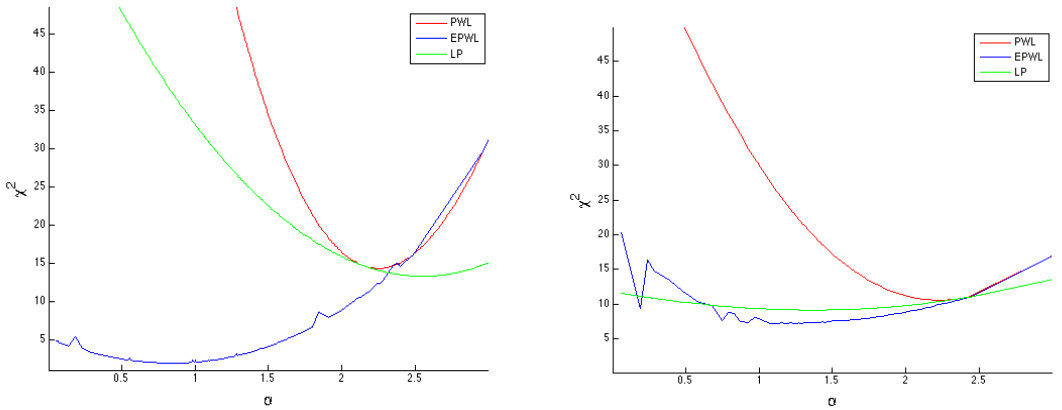

Figure 10: X^2 vs α for 1ES 1959+650 (left) and 1ES 2344+514 (right). In both sources, the EPWL model is a better model for the data.

Source	Model	Minimum χ^2	α	p-value
1ES 1959+650	PWL	28.00	1.63	0.32 %
	EPWL	2.08	0.96	99.57 %
	LP	20.44	1.63	2.54 %
1ES 2344+514	PWL	14.99	1.63	13.24 %
	EPWL	7.21	1.18	61.53%
	LP	9.13	1.37	42.54 %

Table 4: Fitted Model statistics for both sources, finding the minimum χ^2 value with α constrained by H.E.S.S. values.

Source	Model	Minimum χ^2_{red}	α_{min}	Minimum $\chi^2_{red} + 1$	α	δα
1ES 1959+650	PWL	1.31	2.24	2.31	1.69	± 0.55
	EPWL	0.20	0.86	1.20	2.22	± 1.36
	LP	1.34	2.61	2.34	1.45	± 1.16
1ES 2344+514	PWL	1.06	2.23	2.06	1.34	± 0.89
	EPWL	0.80	1.18	1.85	2.97	± 1.79
	LP	1.01	1.37	-	-	-

Table 5: Determining the α parameter and its uncertainty for both sources.

DISCUSSION

For both sources, the most probable model to describe the physics is the EPWL model. However, we can only say that the EPWL applied to 1ES 1959+650 is statistically consistent, as defined by a p-value that is greater than 90%. The reason behind 1ES 2344+514 having two decently large p-values, neither of which is statistically consistent, is due to the larger uncertainty in the Fermi bowtie.

Additionally, sources of similar redshift experience roughly the same attenuation, assuming the EBL is uniformly distributed through the Universe much like the CMB. They should therefore have similar values for the normalization factor α. The results of our α parameter determination show that 1ES 1959+650 and 1ES 2344+514 have consistent attenuation within experimental uncertainty.

CONCLUSION

Based on this analysis, we conclude that the observations by both Fermi and VERITAS are very sensitive to the intrinsic spectrum of the blazar, which is a result of the physics occurring within the jet. Of the three models tested, the EPWL model appears to be the best model for both sources, albeit to different degrees. The results display the inability of simple one-component models, such as PWL and LP models, to accurately and precisely represent the intrinsic flux of the blazars we studied, compared to two-component models like the EPWL. The difference in precision of the Fermi data for 1ES 2344+514 and 1ES 1959+650 is largely responsible for the significant difference in their p-values. With the larger variation in the data for 1ES 2344+514, the fits are less precise, and there is no clear overall 'best' model.

Regardless of the precision for each source, we were able to show that the shape in the measured spectrum is too great to be solely because of the exponential cutoff in the EPWL model. This diminished flux is consistent with our theory of EBL attenuation. Therefore, the noticeable 'kink' seen in the combined Fermi/VERITAS spectrum for both sources is the result of EBL attenuation in the VHE regime.

REFERENCES

1. Biteau, J., Williams, DA., 2015, "*The extragalactic background light, the Hubble constant, and anomalies: conclusions from 20 years of TeV gamma-ray observations,*" Submitted to Astrophysical Journal, arXiv:1502.04166.
2. Holder *et al*., 2006, "*The First VERITAS Telescope*," Astroparticle Physics*,* **25 6**, 391-401.
3. Atwood *et al*., 2009, "*The Large Area Telescope on the Fermi Gamma-ray Space Telescope Mission*," Astrophysical Journal, **697** 1071.
4. Berge *et al*., 2007, "*Background Modelling in Very-High-Energy gamma-ray Astronomy*," Astronomy & Astrophysics*,* **466**, 1219-1229.
5. Nishiyama, T., 1999, "*Detection of a new TeV gamma-ray source of BL Lac object 1ES 1959+650*," Presented at 26th Internation Cosmic Ray Conference, Salt Lake City.
6. Aharonian *et al*., 2004, "*Observations of 54 Active Galactic Nuclei with the HEGRA system of Cherenkov telescopes,*" Astronomy & Astrophysics*,* **421** 529-537.
7. Abramowski, A., *et al*., H.E.S.S. Collaboration, 2013, "*Measurement of the Extragalactic Background Light Imprint on the Spectra of the Brightest Blazars Observed with H.E.S.S.,*" Astronomy & Astrophysics*,* **550 A4.**
8. Franceschini *et al*., 2008, "*The extragalactic optical-infrared background radiations, their time evolution and the cosmic photon-photon opacity*," Astronomy & Astrophysics*,* **487** 837-852.